ACS OMEGA

Open Access



http://pubs.acs.org/journal/acsodf

Article

# Research on the Stability and Response of Food Packaging Polystyrene Resin Materials to γ-ray Irradiation

Jing Yan, Wencai Cheng, Congcong Ding, Ze Qiu, Xiaoan Li, and Xirui Lu*

Cite This: *ACS Omega* 2024, 9, 38668−38677

Read Online

ACCESS | Metrics & More | Article Recommendations | Supporting Information

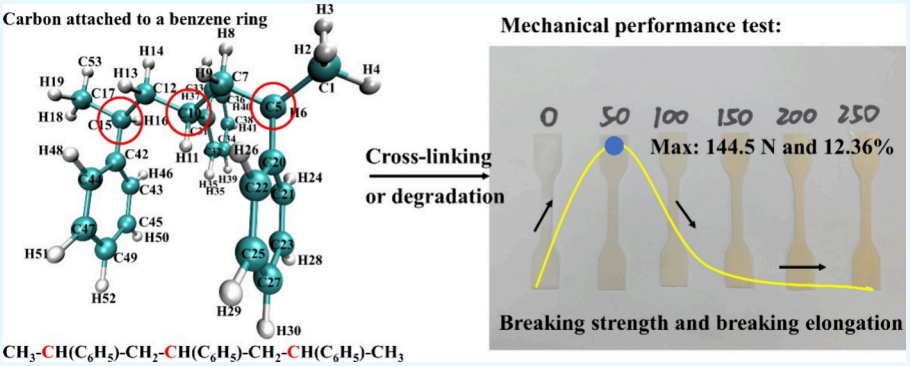


**ABSTRACT:** Radiation stability of food packaging materials is the key to ensuring food quality. In this study, $^{60}Co$ γ-ray was selected to investigate the radiation resistance of food packaging polystyrene (PS) resin material, although the FTIR analysis showed that the intensity of several peaks decreased slightly. The gel permeation chromatography (GPC) results displayed that the value of peak molecular weight (Mp) of PS went from $2.68 \times 10^5$ g/mol down to $2.22 \times 10^5$ g/mol. Moreover, the residual mass (Res) of PS increased from 7.208 to 30.23%, indicating that the tendency of coking of PS was stronger after irradiation. In addition, the peak intensities of the three main pyrolysis products $-CH_2-$, $CH_4$, and $CH_2{=}CH_2$ increased by more than 30% compared to unirradiated PS, and a large number of them were detected in the whole pyrolysis process. Moreover, mechanical property analysis finds that both breaking strength and elongation data increased before irradiation dose of 50 kGy, then, decreased sharply with further increase of irradiation dose. The theoretical bond order analysis confirmed that the tertiary carbon bond attaching the benzene ring had the lowest bond energy. This study can give helpful guidance when using PS for food packing materials.

## 1. INTRODUCTION

Since December 2019, coronavirus disease 2019 (COVID-19), caused by a novel coronavirus (2019-nCoV), has spread worldwide, with enormous social and economic impacts in more than 200 countries worldwide.[1−4] In general, the main mode of transmission of COVID-19 is through respiratory droplets.[5,6] However, the possibility of transmission of the virus through other infected substances (including food and food packaging surfaces) cannot be completely ruled out.[7]

Since early July 2020, at least nine food contamination incidents have been reported across China where 2019-nCoV was found in imported food (mostly packaging).[7] Although different quality checks are carried out at all stages of the food processing and supply chain, taking into account the consumer safety requirements for food packaging as a potential source of further inspection is still particularly necessary. Generally speaking, there are many different processing methods for food processing. Gamma irradiation as an environmentally friendly cold physical process is being used in more than 60 countries worldwide for a variety of socio-economic applications, such as food safety, quarantine, and disinfection of medical supplies and equipment, inactivation of bacteria and viruses in animal sera and biotherapeutics.[8]

Over the past 50 years, polymers have played a crucial role in the development of human society,[9] driving the development of packaging, electronics, automobiles, medical, construction, and many other industries.[10] Polystyrene (PS) is one of the most stable organic polymers, and the presence of a phenyl ($C_6H_5$) group is the key to its properties. These large rings prevent the polymer chains from stacking into a tight crystalline arrangement, so the solid polystyrene is transparent. In addition, the benzene ring limits the rotation of the chain around the carbon−carbon bond, thus making the polymer remarkably rigid.[11] PS is widely used in many aspects of human

Received: May 9, 2024
Revised: August 25, 2024
Accepted: August 28, 2024
Published: September 8, 2024


**Figure 1.** Schematic diagram of a granular PS solid resin sample (a), schematic diagram of a powdered PS sample (100 mesh) (b), and particle size distribution of PS powder after sieving (c).

life and industry because of its low cost, lightweight, ease of manufacture, multifunction, thermal efficiency, durability, and moisture resistance.[12,13]

In general, there are three types of common PS: general polystyrene (GPPS), reinforced polystyrene (HIPS), and expanded polystyrene (EPS). Among them, GPPS is often used to make foamed plastics and thermoplastic-forming materials for food and pharmaceutical packaging due to its high heat resistance temperature, high fluidity (easy-to-blow molding), and almost no additives.[14,15] Moreover, HIPS plastics are produced by blending styrene-butadiene copolymer as an impact modifier and crystal PS (or general-purpose polystyrene, GPPS). It is a common material for packaging refrigerated dairy products.[16] Finally, EPS is a kind of foam crystal polystyrene bead made by adding a foaming agent, which is mainly used in various electrical buffer packaging,[17] food packaging, and live packaging of fresh fish.[18,19] It can be seen that all three kinds of PS materials can be applied in the field of food packaging. However, when it is used as a food packaging material,[20] it is inevitable that PS is sterilized during food processing or during a pandemic to eliminate the source of infection. When irradiation disinfection was selected for application in this field, PS is required to have good irradiation resistance stability.

Therefore, the radiation resistance of PS has also become the first part of our understanding. In 2000, Zhu et al[21] used rapid Ar ion irradiation to chemically modify PS and found that the main chain and benzene ring of PS were destroyed at the core of orbit, at the same time, the material carbonization occurred. Then, in 2008, Singh et al[22] investigated the effect of proton (3 MeV) irradiation on the optical structure of PS and showed that the band gap of UV−vis light of PS was reduced by 27.5%, the absorption intensity of the main characteristic bands in FTIR decreases. In the same year, Liu et al[23] studied the anisotropic deformation of PS particles by using Au ion irradiation. The results showed that the shape of PS particles changed from spherical to elliptical, and the volume of PS particles decreased at the beginning of irradiation; the aspect ratio then increased with the energy density. In 2009, Mathad et al[24] studied the effect of an 8 MeV electron beam on the structure of PS film, and the results showed that the film was resistant to electron beam irradiation in the range of radiation dose studied. In 2022, Cui et al[25] have been applied to evaluate the differences in microplastics (Plastic particles less than 5 mm in diameter) generation behavior of $\alpha$ and $\beta$ crystalline-structured polypropylene ($\alpha$-PP, $\beta$-PP) under conditions of ultraviolet (UV) irradiation and natural forces. The results indicate that after UV aging for 1470−1500 and 1670−1700 h, respectively, $\alpha$-PP generates 71% of microplastics and $\beta$-PP generates 25% of microplastics. In 2023, Huang et al[26] reported a simulation method through associating plastic aging with mechanical failure on a time scale to predict MP generation and give an experimental verification. The results indicate that the proposed evaluation method has high accuracy for predicting MP generation from aged polystyrene foams. Under conditions of ultraviolet (UV) irradiation and heat for 1000 h, the aged polystyrene foam generates significant microplastics ($6.78 \times 10^6$ particles/cm$^3$) by water scouring force after the expected aging time (400 h). In the same year, Ferry et al[27] investigated the effect of the atmosphere on the irradiation of random PS by fast heavy ions. The results showed that PS had a strong resistance to radiation under an inert atmosphere. In addition, the degradation degree of random PS was increased in an oxidizing atmosphere, but the oxidation degree was not high. It could be seen that many researchers had done PS radiation response-related studies.

However, there are few studies of the response mechanism of PS to $^{60}$Co-$\gamma$ rays. In this study, the PS resin is selected as the subject. The radiation resistance and response mechanism are studied by means of SEM, FTIR, XRD, GPC, TG-DSC, TG-MS, and mechanical property analysis. The purpose is to provide a more comprehensive theoretical basis for the application of irradiation technology.

## 2. MATERIAL AND METHODS

**2.1. Materials.** PS $(C_8H_8)_n$ is a colorless, odorless, odorless, tasteless, and glossy transparent granular general-purpose thermoplastic PS resin produced by Shanghai Maclin Biochemical Technology Co., Ltd. The digital images are shown in Figure 1. To facilitate test characterization and increase radiation exposure rates, the PS resin, as shown in Figure 1a was crushed by a high-speed mill. Then, using the GB/T6003.1−2002 standard sieve (100 mesh) to handle them, the small particles, as shown in Figure 1b were obtained. Moreover, a more detailed sample handling procedure is displayed in Figure S1 (Supporting Information). In addition, Figure 1c shows the particle size distribution of PS powder after sieving. Similarly, the particle size distribution test raw data are shown in Table S1 (Supporting Information). The $^{60}$Co source was a cylindrical $\gamma$-ray source, and it was supplied by China Gold Irradiation Chengdu Co., Ltd.


https://doi.org/10.1021/acsomega.4c04407
ACS Omega 2024, 9, 38668−38677

**2.2. Irradiation Experimental Method.** The samples of PS with sufficient doses of 0, 50, 100, 150, 200, and 250 kGy were prepared and sent to China Gold Irradiation Chengdu, LTD for irradiation treatment. The irradiation dose is the product of the irradiation time and irradiation intensity (the irradiation dose rate). In this study, the cumulative radiation dose was investigated, so the dose rate was set at 10 kGy/6 h, and different doses were processed at different times. Therefore, the irradiation time was set at 0, 30, 60, 90, 120, and 150 h for the samples at six dose points of 0, 50, 100, 150, 200, and 250 kGy, respectively. The final test was carried out after irradiation treatment.

**2.3. Sample Characterization.** The particle size distribution of the original PS powder was measured by a laser particle size analyzer (MS3000, Malvern, Britain). The microstructure of PS was observed by scanning electron microscopy (SEM, TM4000, Japan). The detailed structural characteristics of PS were tested by X-ray diffraction (XRD, Empyrean, Netherlands) and Fourier transform infrared spectrometer (FTIR, Spectrum One, USA). In addition, the molecular weight changes of PS were observed using gel permeation chromatography (GPC, Agilent PL-GPC220, USA. Test conditions: trichlorobenzene (high temperature); detector: refractive index detector; chromatographic column: PLgel-MIXED-BLS300 × 7.5mmx2; flow rate: 1 mL/min; standard product: PS (polystyrene); experimental temperature: 150 °C; mobile phase: TCB (1,2, 4-trichlorobenzene)). Also, the tests of GPC were conducted by Shiyanjia Lab (www.shiyanjia.com). Thermal characteristic was analyzed by a synchronous thermal analyzer (TG-DSC, Netzsch STA 449 F3, Germany, air atmosphere) and thermogravimetric mass spectrometry (TG-MS, Netzsch STA 449 F3, Germany, air atmosphere. Heating rate: 10 °C/min; MS detection range: 1−300).

In addition, the mechanical properties of PS samples were tested according to "GBT 10400.1−2018 Determination of tensile properties of plastics Part 1: General Principles" and "GBT 10400.3−2006 Determination of tensile properties of plastics Part 3: Test conditions for films and sheets". The shape of the sample in the test is dumbbell type, and its sample size is shown in Figure 2. Specifically, the mechanical properties test sample was obtained by melting and shaping the irradiated PS powder sample into a dumbbell compression groove mold in the tensile test laboratory. The specific production process is shown in Figure S2 (Supporting Information).

Finally, the Multiwfn procedure[28] and Gaussian software were used to assist the electron localization function (ELF)[29,30] and Laplacian bond order (LBO) analysis[31] to clarify the irradiation degradation mechanisms.

## 3. RESULTS AND DISCUSSION

**3.1. Structure and Phase Analysis.** We carried out the structure and the phase change analysis by FTIR and XRD. Before discussing the FTIR results of PS, it is pertinent to consider the structure. The structure of the polymer-repeating unit can be represented as $[CH_2C(C_6H_5)H]_n$.[32] The presence of the phenyl ($C_6H_5$) groups is key to the properties of polystyrene. These large rings prevent the polymer chains from packing into close crystalline arrangements so that solid polystyrene is transparent. The chain is probably stiffened somewhat as a result of the interference between neighboring phenyl groups, but there is an indication[33] that no regularity exists along the carbon backbone. In addition, the phenyl rings

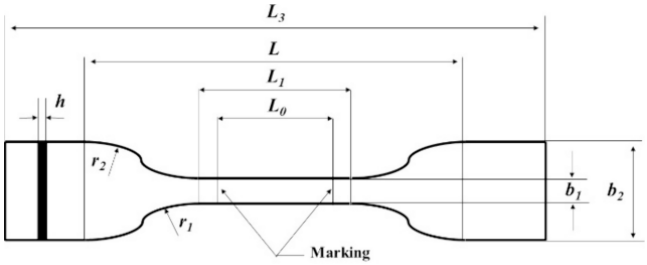


$b_1$—Narrow parallel section width: 6 mm ± 0.4 mm;

$b_2$—End width: 25 mm ± 1 mm;

h—Thickness: ≤1 mm;

$L_0$—Marking length: 25 mm ± 0.25 mm;

$L_1$—The length of the narrow parallel part: 33 mm ± 2mm;

L—Initial distance between fixtures: 80 mm ± 5 mm;

$L_3$—Overall length: ≥ 115 mm;

$r_1$—Minor radius: 14 mm± 1 mm;

$r_2$—Smooth radius: 25 mm± 2 mm.

**Figure 2.** Schematic diagram of sample shape and size for mechanical properties analysis and testing of PS.

restrict the rotation of the chains around the carbon−carbon bonds, thus lending the polymer its noted rigidity.

The FTIR and XRD results are shown in Figure 3 and Table 1. FTIR spectrum analysis shows that the intensity of some characteristic peaks in the FTIR spectrum has a slight weakening change. The change of characteristic peaks formed by the out-of-plane unsaturation C−H symmetric bending vibration at 754.00 and 695.00 $cm^{-1}$ are quite significant, especially at high irradiation doses. This indicates that although PS resin has a certain radiation resistance in the range of radiation dose studied, with the increase of radiation dose, the damage of γ-rays to PS is still slightly increased.

Finally, the XRD test results are listed in Figure 3c. The XRD results of the original sample and the samples at different irradiation doses demonstrate that the polymers are completely amorphous. This is mainly due to the random orientation of the phenyl group.[34,35]

**3.2. Molecular Weight Change Analysis.** Irradiation mainly caused cross-linking and degradation effects for polymers.[43,44] The most immediate result shows a change in the molecular weight. The molecular weight change of PS is shown in Figure 4. The values of Mp, Mn, Mw, and PDI are given in Table 2. Seeing from Table 2 and Figure 4a, the Mp value of PS decreases from 2.68 × $10^5$ g/mol down to 2.22 × $10^5$ g/mol with the increase in irradiation dose. In addition, the Mn value decreases after a 100 kGy irradiation dose and then increases with the dose. Furthermore, Mw shows a slight increase from 3.37 × $10^5$ to 3.56 × $10^5$ g/mol. From the molecular weight distribution statistics in Figure 4c, it can be seen that the main reason for this change is that the molecular weight greater than 1.00 × $10^6$ g/mol increases with the increase of irradiation dose.

Moreover, after exposure to a dose of 100 kGy, the increase is from 24.5 to 29.4% in the molecular weight range of 0.10−1.00 × $10^5$ g/mol and the decrease is from 24.5 to 21.7% in the molecular weight range of 2.00−4.00 × $10^5$ g/mol. These show that the cross-linking and degradation effects occur at the same time. This is also the reason why Mn decreases first and then increases with the increase of the irradiation dose. Finally, PDI is a parameter used to measure the molecular weight


https://doi.org/10.1021/acsomega.4c04407
ACS Omega 2024, 9, 38668−38677

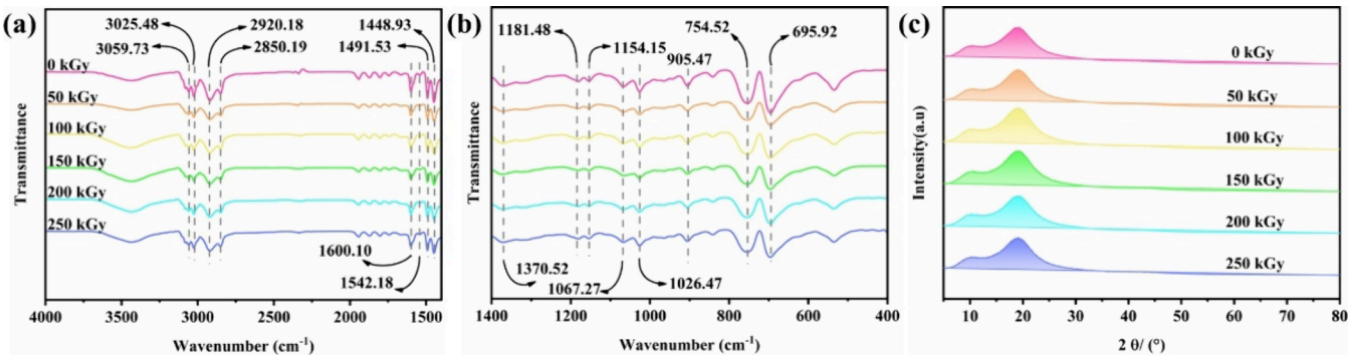


**Figure 3.** FT-IR spectra of PS at different irradiation doses (a, b). XRD spectra of PS at different irradiation doses (c).

**Table 1. FTIR Test Results of PS**

| wavenumber ($cm^{-1}$) | functional group | references |
|---|---|---|
| 3059.73, 3025.48 | aromatic C−H stretching | 36 |
| 2920.18 | $-CH_2-$ asymmetrical stretching | 37 |
| 2850.19 | $-CH_2-$ symmetrical stretching | 38,39 |
| 1600.10, 1542.18, 1491.53, 1448.93 | benzene ring skeleton vibration | 36 |
| 1370.52 | $CH_3$ groups | 36,40 |
| 1181.48, 1154.15, 1067.27, 1026.47 | $-CH_2-$ out-of-plane bending, aromatic C−H in-plane bending | 41 |
| 905.47, 754.00, 695.00 | aromatic C−H out-of-plane bending | 36,41,42 |

distribution breadth of polymers. The larger the PDI value, the wider the molecular weight distribution.[45] It can be seen from Table 2 that the PDI value of PS increases after irradiation, indicating a wider molecular weight distribution. The molecular weight distribution in Figure 4b also illustrates this. In general, the cross-linking and degradation effects of PS by $\gamma$-ray irradiation are simultaneous. Also, the final effect of irradiation is the widening of the molecular weight distribution of PS. Also, the larger the irradiation dose, the more dispersed the molecular weight distribution.

**3.3. Thermal Stability.** To evaluate the effect of irradiation on its thermal stability, thermogravimetric analysis was carried out at 10 °C/min. Figure 5a,b displays the TG-DTG curves of PS. The degradation of the contrast PS commences at 229.93 °C attains its maximum at 489.41 °C and ends at 562.67 °C. At low temperatures, products mainly consist of liquid compounds (monoaromatic). At higher temperatures, gas and coke yields are higher and the liquid fraction has significant aromatics (dimer, trimer).[46−48] Thus, the thermal decomposition of PS mainly proceeds through two processes. The two processes are labeled first and second.

**Table 2. GPC Results for PS (0, 100, and 200 kGy)[a]**

| irradiation dose (kGy) | Mp (g/mol) | Mn (g/mol) | Mw (g/mol) | PDI |
|---|---|---|---|---|
| 0 | $2.68 \times 10^5$ | $8.93 \times 10^4$ | $3.37 \times 10^5$ | 3.78 |
| 100 | $2.48 \times 10^5$ | $7.79 \times 10^4$ | $3.38 \times 10^5$ | 4.35 |
| 200 | $2.22 \times 10^5$ | $7.87 \times 10^4$ | $3.56 \times 10^5$ | 4.52 |

[a]Mp is the peak molecular weight, the highest molecular weight of the molecular retention time curve; Mn is the number of average molecular weight, weighted by the number of statistical molecular weight results:$Mn = (\sum_i n_i M_i)/(\sum_i n_i) = \sum_i N_i M_i$;Mw is the weight average molecular weight; mass as the weight statistical molecular weight results: $Mw = (\sum_i n_i M_i^2)/(\sum_i n_i M_i) = (\sum_i w_i M_i)/(\sum_i w_i) = \sum_i W_i M_i$; PDI is the polydispersity index; ratio of weight average molecular weight to number average molecular weight: PDI = Mw/Mn.

The ending temperature of the first (from 489.41 down to 461.99 °C) and second (from 562.67 down to 525.43 °C) decrease after irradiation, and the hump deformation formed by the second widens greatly. Meanwhile, the maximum weight loss rate temperature also decreases from 453.74 to 433.59 °C. Therefore, the pyrolysis of PS becomes easier after irradiation. Furthermore, Figure 5 displays that the residual mass (Res) from the pyrolysis of unirradiated PS is 7.208%, while the irradiated sample is up to 30.23%. Therefore, no matter whether the PS samples are irradiated or not, the PS samples have a tendency of coking,[49] while the tendency of coking was stronger after irradiation. This should be related to the molecular content of molecular weight greater than $1.00 \times 10^6$ g/mol increases found in the GPC analysis.

Figure 5c,d illustrates the DSC curves for PS during the pyrolysis process. The DSC curve of PS can distinguish approximately 3 temperature regions. In region I, the thermal effect is endothermic. This enthalpy of absorption is related to

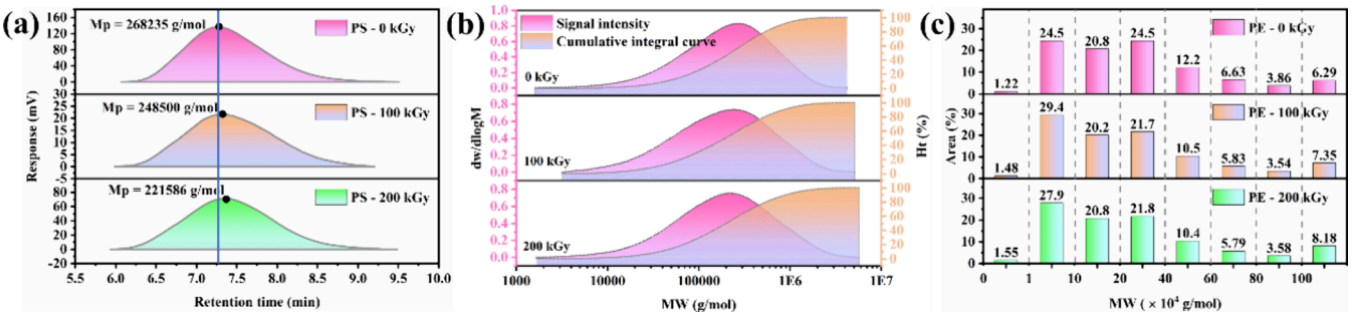


**Figure 4.** Molecular retention time curves (a). Molecular weight distribution curves (b). Statistical result of the molecular weight distribution (c).



https://doi.org/10.1021/acsomega.4c04407
ACS Omega 2024, 9, 38668−38677

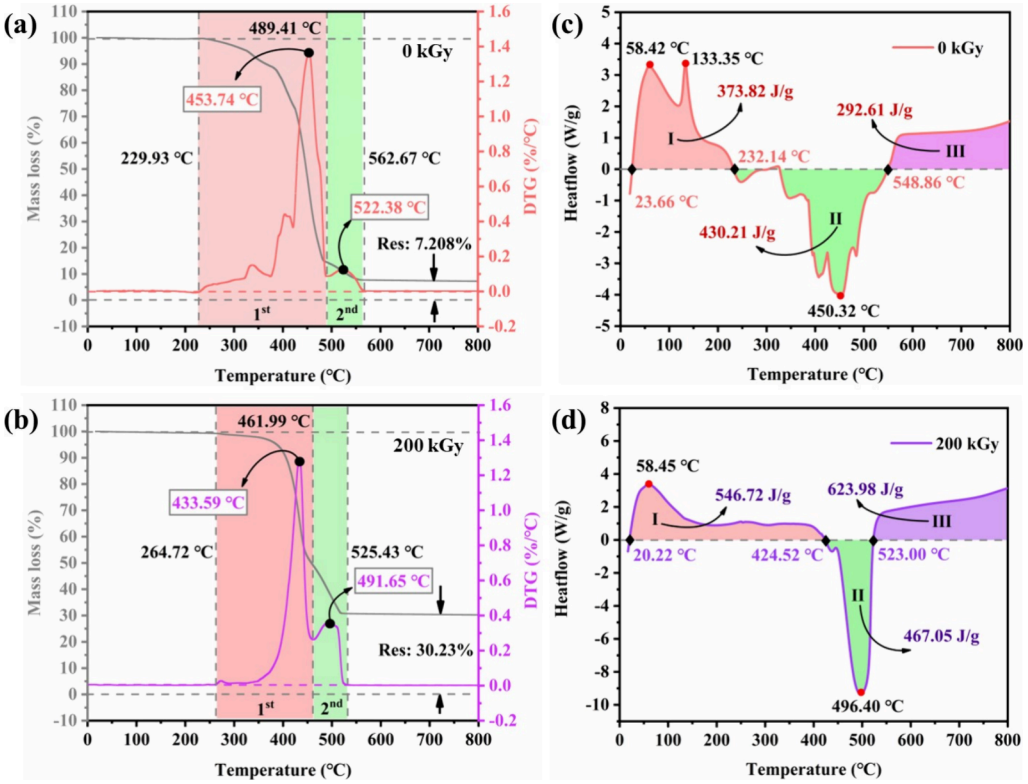


**Figure 5.** TG-DTG curves of PS: (a) 0 kGy; (b) 200 kGy. DSC curves of PS: (c) 0 and (d) 200 kGy.

the heat absorbed by the phase transition (melting) and the beginning of decomposition (i.e., the competition between intramolecular and intermolecular bond breaking) of PS; in region II, the thermal effect is exothermic, and the polymer weight loss mainly occurs in this region, so the exothermic effect in this region is mainly caused by the forging chain decomposition during PS decomposition. The thermal effect of the last stage III is endothermic, in which the weight loss is very low and gasification and coking are the main reactions. After irradiation, the absorption and release of heat in all three regions of PS increased by 46.25, 8.56, and 113.25% espectively. It is concluded that the molecular content of molecular weight greater than $1.00 \times 10^6$ g/mol increases and the increase of coking tendency after irradiation have a great influence on the endothermic and exothermic effects of PS pyrolysis.

The MS detection results are shown in Figure 6, which intuitively shows the distribution of pyrolysis gas-phase products of PS. It is clear from Figure 6a,b that the products are mainly distributed in the low molecular weight stage, and the characteristic peak intensity of each pyrolysis product molecule increases significantly after irradiation. Furthermore, molecules in the charge/mass ratio ($m/z$) range from 0 to 50 are plotted separately, as shown in Figure 6c,d. The main volatile products with $m/z$ values of 14, 16, and 28 are $-CH_2-$, $CH_4$, and $CH_2{=}CH_2$, respectively. In addition, small amounts of $H_2O$ and $CO_2$ with $m/z$ of 18 and 44 were also detected. After irradiation, the peak intensities of $-CH_2-$, $CH_4$, and $CH_2{=}CH_2$ increased by 30.47, 38.67, and 36.24% of unirradiated PS, respectively. In addition, the intensity of the characteristic peak of $O_2$ left behind after the reaction in the reaction system increased. (These indicate that the oxygen consumption of PS pyrolysis is reduced after irradiation.) Finally, the distributions of $-CH_2-$, $CH_4$, and $CH_2{=}CH_2$ molecules with temperature are shown in Figure 6e,f. Before irradiation, the three main products of PS are mainly detected in the range of 300−400 °C, while after irradiation, a large number of them are detected in the whole range of pyrolysis temperature. It is shown that the thermal stability of PS material after irradiation will decrease greatly in practical applications, and $CH_4$ and $CH_2{=}CH_2$ are easily produced by slight heating. Therefore, the practical application potential of PS material after irradiation will be greatly reduced.

**3.4. Mechanical Performance Analysis.** The microscopic images at different irradiation doses of PS are shown in Figure 7. It is obvious that the micromorphology of PS has little change after irradiation. However, the irradiation effect causes the samples to transform color from white to orange-yellow obviously (Figure 8a). The mechanical performance test results for PS are shown in Figure 8, and the raw data plot is shown in Figures S3−S8 (Supporting Information). Figure 8a−d shows schematic diagrams of the samples, and Figure 8e,f shows the curves of PS breaking strength and breaking elongation as the irradiation dose increases, respectively. It is obvious from Figure 8e,f that the two parameters have curves of PS breaking strength and breaking elongation as the irradiation dose increases, with similar variation laws. When the irradiation dose is below 50 kGy, it increases first with the increase of irradiation dose and then decreases when the irradiation dose reaches 50 kGy with the further increase of irradiation dose. Both breaking strength and breaking elongation reach the maximum value at 50 kGy: 144.50 N and 12.36%, respectively.

According to the above analysis, irradiation has two effects on PS: cross-linking and degradation. Therefore, it is believed that when the irradiation dose is lower than 50 kGy, the cross-


https://doi.org/10.1021/acsomega.4c04407
ACS Omega 2024, 9, 38668−38677

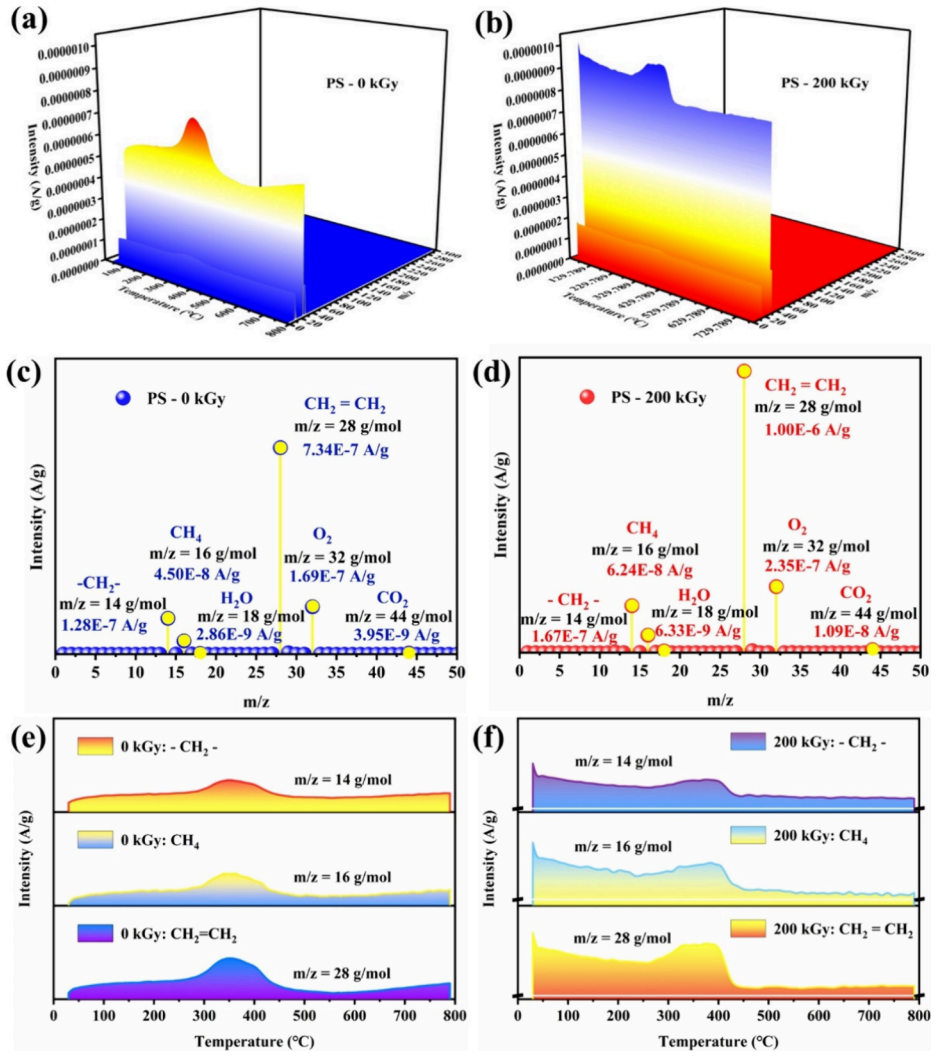


**Figure 6.** 3D MS diagrams of gas product distribution of PS: (a) 0 and (b) 200 kGy. The maximum intensity of characteristic peak of each $m/z$ product was detected in the range of 0−50 $m/z$: (c) 0 and (d) 200 kGy. Distribution of molecules with $m/z$ ratios of 14, 16, and 28 with the temperature changing: (e) 0 and (f) 200 kGy.

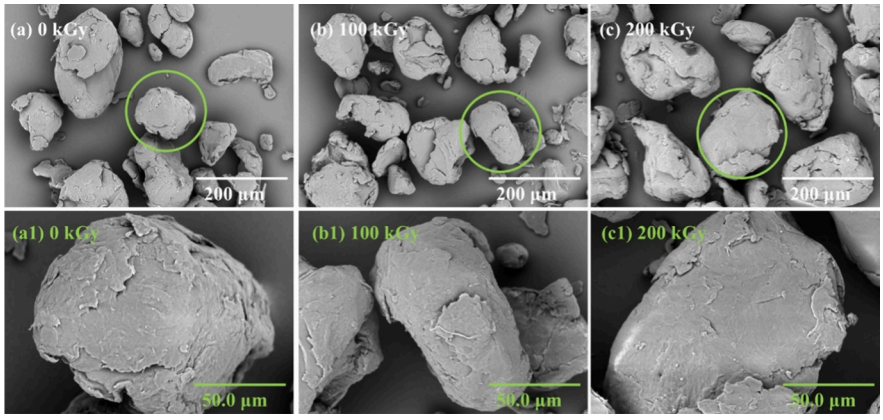


**Figure 7.** SEM images of PS at different irradiation doses (a−c); locally magnified image of some PS particles (a1−c1).

linking effect of irradiation on PS is stronger, which enhances its mechanical properties. With the further increase of the irradiation dose, the degradation effect is dominant, which leads to the decrease of mechanical properties of the sample. In general, the decrease of breaking strength and elongation at break after the irradiation dose reaches 100 kGy is consistent with the above conclusion that the performance of PS decreases after the irradiation dose of 100 and 200 kGy.

**3.6. Analysis of Irradiation Effect Mechanisms Based on ELF and LBO.** The electron cloud density distributions of PS are shown in Figure 9a and Figure S9 (Supporting Information). In the projection shown in the image, the darker


https://doi.org/10.1021/acsomega.4c04407
ACS Omega 2024, 9, 38668−38677

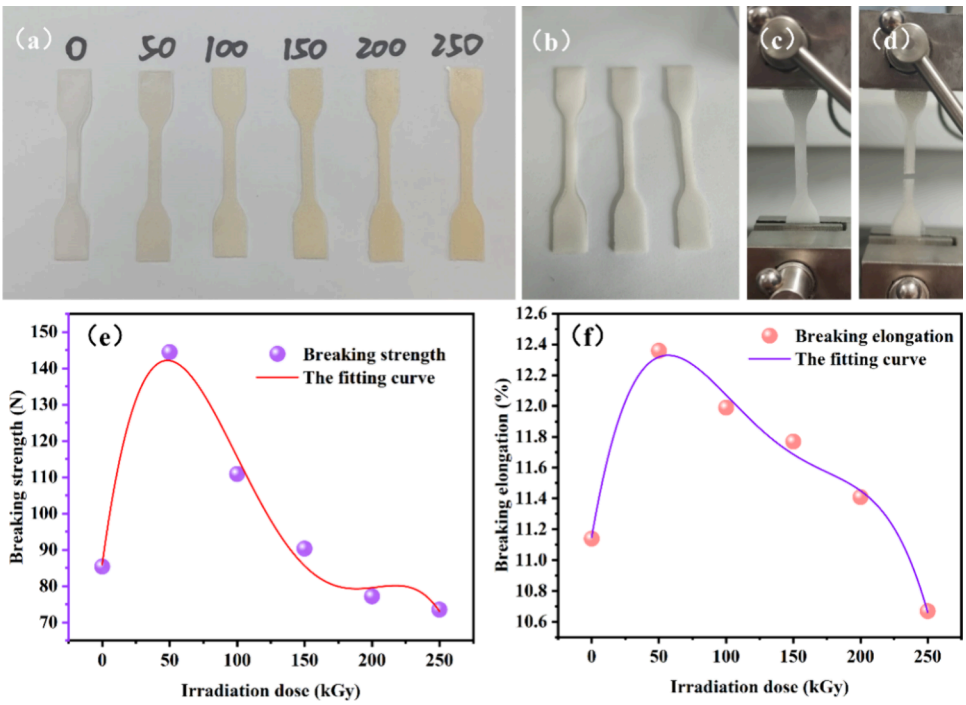


**Figure 8.** Schematic diagram of the tensile test sample: (a) prepared at different irradiation doses, (b) three parallel samples prepared for the original sample (0 kGy); (c) clamped on the testing machine before the test; (d) broken on the testing machine after the test; change curve of PS breaking strength with the increase of irradiation dose (e); change curve of PS breaking elongation with the increase of irradiation dose (f).

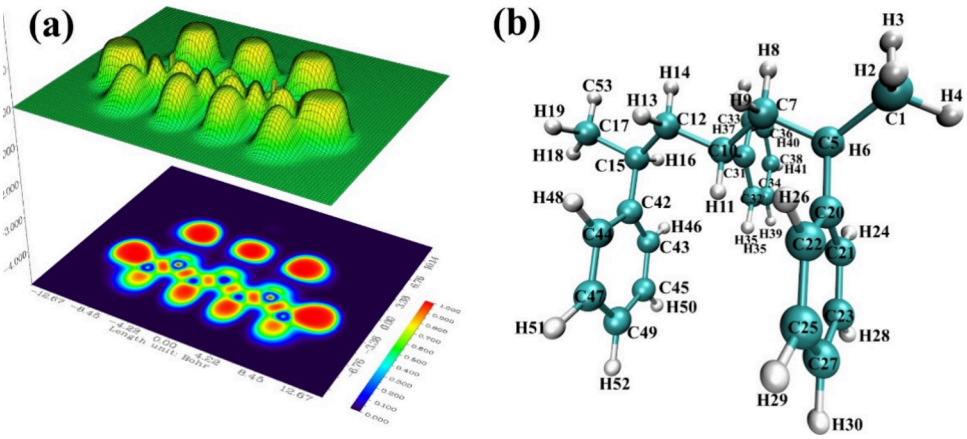


**Figure 9.** PS molecule example: $CH_3-CH(C_6H_5)-CH_2-CH(C_6H_5)-CH_2-CH(C_6H_5)-CH_3$: (a) electron cloud density distribution, (b) ball-and-stick model.

the red, the denser the electron cloud. The stick model is shown in Figure 9b, and the corresponding atoms are labeled. Moreover, LBO can be used to measure the strength of the chemical bonds. Also, the LBO of each chemical bond in PS is listed in Table 3. In the example PS molecule, the C−C bonds with the lowest LBO values are C7−C10 and C10−C12, both 0.897, indicating that these are the most easily broken. Then, the LBO value of C5−C7 and C12−C15 is 0.900. All C−C bonds that are mentioned before are formed by the involvement of the tertiary carbon attaching the benzene ring. It is because these C−C bonds break. The cross-linking and degradation of PS are realized, resulting in changes in molecular weight. In addition, the C−H bonds with the lowest LBO value are C5−H6, C7−C8, C7−H9, C10−H11, C12−H13, C12−H14, and C15−H16. These C−H bonds are formed by the secondary and tertiary carbon involvement, which are located in the main chain.

Generally speaking, $\beta$-cleavage is the most frequent reaction during the degradation of PS.[50] There are two forms: the free radical break at the end of the chain and the free radical break in the chain. The former is the process of PS depolymerization, which is a reversible process (also can be cross-linked). In the process, the self-scission of PS fragment radical accelerates the midchain and end chain $\beta$-scission by attacking the polymer chain by a phenyl radical. This reaction ends in the formation of styrene and end-chain free radicals. The attack of free radicals on the secondary (C5, C10, C15) and tertiary carbons (C7, C12) by $\beta$-scission immediately forms the oligomers of styrene.[50] This is the main way for PS degradation and cross-linking.


https://doi.org/10.1021/acsomega.4c04407
ACS Omega 2024, 9, 38668−38677

Table 3. LBO Values of the Chemical Bonds in the PS Molecule, for Example

| chemical bond | LBO value | chemical bond | LBO value | chemical bond | LBO value | chemical bond | LBO value |
|---|---|---|---|---|---|---|---|
| C1−C5 | 0.921 | C25−C27 | 1.494 | C1−H2 | 0.829 | C22−H26 | 0.854 |
| C5−C7 | 0.900 | C31−C32 | 1.445 | C1−H3 | 0.827 | C23−H28 | 0.861 |
| C5−C20 | 0.974 | C31−C33 | 1.457 | C1−H4 | 0.836 | C25−H29 | 0.860 |
| C7−C10 | 0.897 | C32−C34 | 1.496 | C5−H6 | 0.818 | C27−H30 | 0.861 |
| C10−C12 | 0.897 | C33−C36 | 1.492 | C7−H8 | 0.814 | C32−H35 | 0.855 |
| C10−C31 | 0.969 | C34−C38 | 1.493 | C7−H9 | 0.814 | C33−H37 | 0.862 |
| C12−C15 | 0.900 | C36−C38 | 1.502 | C10−H11 | 0.814 | C34−H39 | 0.862 |
| C15−C17 | 0.921 | C42−C43 | 1.446 | C12−H13 | 0.814 | C36−H40 | 0.862 |
| C15−C42 | 0.974 | C42−C44 | 1.459 | C12−H14 | 0.814 | C38−H41 | 0.859 |
| C20−C21 | 1.459 | C43−C45 | 1.496 | C15−H16 | 0.818 | C43−H46 | 0.854 |
| C20−C22 | 1.445 | C44−C47 | 1.490 | C17−H18 | 0.827 | C44−H48 | 0.855 |
| C21−C23 | 1.490 | C45−C49 | 1.494 | C17−H19 | 0.829 | C45−H50 | 0.860 |
| C22−C25 | 1.496 | C47−C49 | 1.503 | C17−H53 | 0.836 | C47−H51 | 0.861 |
| C23−C27 | 1.503 | | | C21−H24 | 0.855 | C49−H52 | 0.861 |

## 4. CONCLUSIONS

In this work, the irradiation resistance of PS irradiated by γ-rays in the range 0−250 kGy was investigated. The GPC results displayed that Mp value of PS went from $2.68 \times 10^5$ g/mol down to $2.22 \times 10^5$ g/mol. In this process, the molecular content of molecular weight greater than $1.00 \times 10^6$ g/mol increased, resulting in the increase of Mw. The results of thermal stability analysis showed that the pyrolysis process of PS has two main stages. The mechanical properties analysis showed that the PS has a maximum inflection point at 50 kGy. Eventually, the theoretical bond order analysis confirmed that the tertiary carbon bond attaching the benzene ring had the lowest bond energy. In conclusion, the results of this study give helpful guidance when using PS for food packing materials.

## ■ ASSOCIATED CONTENT

### Supporting Information

The Supporting Information is available free of charge at https://pubs.acs.org/doi/10.1021/acsomega.4c04407.

More detailed powder sample handling procedure; particle size; more detailed sample handling procedure of the mechanical properties test; results of theoretical calculations; GPC data (PDF)

## ■ AUTHOR INFORMATION


### Corresponding Author

**Xirui Lu** − *State Key Laboratory of Environment-Friendly Energy Materials and National Co-innovation Center for Nuclear Waste Disposal and Environmental Safety, Southwest University of Science and Technology, Mianyang 621010, P. R. China; Tianfu Institute of Research and Innovation, Southwest University of Science and Technology, Chengdu 610299, P. R. China;* orcid.org/0000-0003-4751-8408; Email: luxiruimvp116@163.com

### Authors

**Jing Yan** − *State Key Laboratory of Environment-Friendly Energy Materials and National Co-innovation Center for Nuclear Waste Disposal and Environmental Safety, Southwest University of Science and Technology, Mianyang 621010, P. R. China*

**Wencai Cheng** − *State Key Laboratory of Environment-Friendly Energy Materials and National Co-innovation Center for Nuclear Waste Disposal and Environmental Safety, Southwest University of Science and Technology, Mianyang 621010, P. R. China; Tianfu Institute of Research and Innovation, Southwest University of Science and Technology, Chengdu 610299, P. R. China;* orcid.org/0000-0001-8912-3004

**Congcong Ding** − *State Key Laboratory of Environment-Friendly Energy Materials and National Co-innovation Center for Nuclear Waste Disposal and Environmental Safety, Southwest University of Science and Technology, Mianyang 621010, P. R. China; Tianfu Institute of Research and Innovation, Southwest University of Science and Technology, Chengdu 610299, P. R. China*

**Ze Qiu** − *State Key Laboratory of Environment-Friendly Energy Materials and National Co-innovation Center for Nuclear Waste Disposal and Environmental Safety, Southwest University of Science and Technology, Mianyang 621010, P. R. China*

**Xiaoan Li** − *Nuclear Medicine Laboratory of Mianyang Central Hospital, Mianyang 621010, P. R. China*

Complete contact information is available at: https://pubs.acs.org/10.1021/acsomega.4c04407


### Notes

The authors declare no competing financial interest.

## ■ ACKNOWLEDGMENTS

The authors appreciate the financial support from the Project of State Key Laboratory of Environment-friendly Energy Materials, Southwest University of Science and Technology (no. 22fksy12), the Open Foundation of NHC Key Laboratory of Nuclear Technology Medical Transformation (Mianyang Central Hospital) (2021HYX028), the Foundation from Tianfu Institute of Research and Innovation (2022ZY013), and the Sichuan Science and Technology Program (2022NSFSC1197).

## ■ REFERENCES

(1) Mutters, N. T.; Malek, V.; Agnandji, S. T.; Günther, F.; Tacconelli, E. Evaluation of the scientific impact of the Ebola epidemic: a systematic review. *Clinical Microbiology and Infection.* **2018**, *24*, 573−576.

(2) Tanaka, S. Economic Impacts of SARS/MERS/COVID-19 in Asian Countries. *Asian Econ. Policy Rev.* **2021**, *17*, 41−61.

(3) Long, J. A.; Ren, C. Associations between mobility and socio-economic indicators vary across the timeline of the Covid-19 pandemic. *Comput. Environ. Urban Syst.* **2022**, *91*, No. 101710.
(4) Profeta, A.; Siddiqui, S. A.; Smetana, S.; Hossaini, S. M.; Heinz, V.; Kircher, C. The impact of Corona pandemic on consumer's food consumption. *Journal of Consumer Protection and Food Safety.* **2021**, *16*, 305−314.
(5) Manigandan, S.; Wu, M. T.; Ponnusamy, V. K.; Raghavendra, V. B.; Pugazhendhi, A.; Brindhadevi, K. A systematic review on recent trends in transmission, diagnosis, prevention and imaging features of COVID-19. *Process Biochemistry.* **2020**, *98*, 233−240.
(6) Wilson, A. M.; Sleeth, D. K.; Schaefer, C.; Jones, R. M. Transmission of Respiratory Viral Diseases to Health Care Workers: COVID-19 as an Example. *Annual Review of Public Health.* **2022**, *43*, 311−330.
(7) Han, J.; Zhang, X.; He, S.; Jia, P. Can the coronavirus disease be transmitted from food? A review of evidence, risks, policies and knowledge gaps. *Environmental Chemistry Letters.* **2021**, *19* (1), 5−16.
(8) Jinia, A. J.; Sunbul, N. B.; Meert, C. A.; Miller, C. A.; Clarke, S. D.; Kearfott, K. J.; Matuszak, M. M.; Pozzi, S. A. Review of sterilization techniques for medical and personal protective equipment contaminated with SARS-CoV-2. *IEEE Access.* **2020**, *8*, 111347−111354.
(9) Geyer, R.; Jambeck, J. R.; Law, K. L. Production, use, and fate of all plastics ever mad. *Sci. Adv.* **2017**, *3* (7), No. e1700782.
(10) Maafa, I. M. Pyrolysis of Polystyrene Waste: A Review. *Polymers.* **2021**, *13* (2), 225.
(11) Birkinshaw, C.; Buggy, M.; O'Neill, M. Fracture of Irradiated Polystyrene. *J. Appl. Polym. Sci.* **1990**, *41* (7−8), 1913−1921.
(12) Singh, L.; Samra, K. S.; Singh, R.; Solania, I.; Avasthi, D. K. Degradation of nickel (86MeV) ion irradiated polystyrene. *Journal of Non-Crystalline Solids.* **2008**, *354* (1), 41.
(13) Capricho, J. C.; Prasad, K.; Hameed, N.; Nikzad, M.; Salim, N. Upcycling Polystyrene. *Polymers.* **2022**, *14* (22), 5010.
(14) Howell, B. A. The utilization of TG/GC/MS in the establishment of the mechanism of poly(styrene) degradation. *Journal of Thermal Analysis and Calorimetry.* **2007**, *89*, 393−398.
(15) Welle, F. Diffusion Coefficients and Activation Energies of Diffusion of Organic Molecules in Polystyrene below and above Glass Transition Temperature. *Polymers.* **2021**, *13* (8), 1317.
(16) Guazzotti, V.; Hendrich, V.; Gruner, A.; Fiedler, D.; Störmer, A.; Welle, F. Migration of Styrene in Yogurt and Dairy Products Packaged in Polystyrene: Results from Market Samples. *Foods.* **2022**, *11* (14), 2120.
(17) An, X.; Huang, B.; Shi, D. Cushioning properties and application of expanded polystyrene for a dynamic nonlinear system. *Eng. Rep.* **2023**, *5* (9), No. e12648.
(18) Loddo, V.; Marcì, G.; Palmisano, G.; Yurdakal, S.; Brazzoli, M.; Garavaglia, L.; Palmisano, L. Extruded expanded polystyrene sheets coated by $TiO_2$ as new photocatalytic materials for foodstuffs packaging. *Appl. Surf. Sci.* **2012**, *261*, 783−788.
(19) Rodríguez-Liébana, J. A.; Martín-Lara, M. A.; Navas-Martos, F. J.; Peñas-Sanjuan, A.; Godoy, V.; Arjandas, S.; Calero, M. Morpho-structural and thermo-mechanical characterization of recycled polypropylene and polystyrene from mixed post-consumer plastic waste. *Journal of Environmental Chemical Engineering.* **2022**, *10* (5), No. 108332.
(20) Singh, L.; Samra, K. S.; Singh, R.; Kumar, R. Proton Irradiated Polystyrene as a Food Packaging Material. *J. Plastic Film Sheeting.* **2007**, *23* (4), 285.
(21) Zhu, Z.; Jin, Y.; Liu, C.; Sun, Y.; Hou, M.; Zhang, C.; Wang, Z.; Liu, J.; Chen, X.; Li, B.; Wang, Y. Chemical modifications of polystyrene under swift Ar ion irradiation: A study of the energy loss effects. *Nuclear Instruments and Methods in Physics Research Section B: Beam Interactions with Materials and Atoms.* **2000**, *169* (1−4), 83−88.
(22) Singh, L.; Singh Samra, K. Opto-structural characterization of proton (3 MeV) irradiated polycarbonate and polystyrene. *Radiat. Phys. Chem.* **2008**, *77* (3), 252−258.
(23) Liu, Y.; Zhao, Z.; Chen, Y.; Lan, D.; Wang, Y. Anisotropic deformation of polystyrene particles by MeV Au ion irradiation. *Nuclear Instruments and Methods in Physics Research Section B: Beam Interactions with Materials and Atoms.* **2008**, *266* (6), 894−898.
(24) Mathad, R. D.; Kumar, H. G. H.; Sannakki, B.; Ganesh, S.; Sarma, K. S. S.; Badiger, M. V. High energy electron irradiation effects on polystyrene films. *Radiat. Effects Defects Solids.* **2009**, *164* (10), 656.
(25) Cui, Q.; Yang, X.; Li, J.; Miao, Y.; Zhang, X. Microplastics generation behavior of polypropylene films with different crystalline structures under UV irradiation. *Polym. Degrad. Stab.* **2022**, *199*, No. 109916.
(26) Huang, Z.; Cui, Q.; Yang, X.; Wang, F.; Zhang, X. An evaluation model to predict microplastics generation from polystyrene foams and experimental verification. *Journal of Hazardous Materials.* **2023**, *446*, No. 130673.
(27) Ferry, M.; Cornaton, M.; Durand, D.; Esnouf, S.; Aymes-Chodur, C.; Ngono, Y. Atmosphere and dose effects on the SHI irradiation of atactic polystyrene. *Radiat. Phys. Chem.* **2023**, *212*, No. 111135.
(28) Lu, T.; Chen, F. Multiwfn: A multifunctional wavefunction analyzer. *J. Comput. Chem.* **2012**, *33*, 580−592.
(29) Pramila, M. J.; Dhas, D. A.; Joe, I. H.; Balachandran, S.; Vinitha, G. Structural insights, spectral, flourescence, Z-scan, C-H···O/N-H···O hydrogen bonding and AIM, RDG, ELF, LOL, FUKUI analysis, NLO activity of N-2(Methoxy phenyl) acetamide. *J. Mol. Struct.* **2023**, *1272*, No. 134140.
(30) Potla, K. M.; Poojith, N.; Osório, F. A. P.; Valverde, C.; Chinnam, S.; Suchetan, P. A.; Vankayalapati, S. An analysis of spectroscopic, computational and biological activity studies of L-shaped sulfamoylbenzoic acid derivatives: A third order nonlinear optical material. *J. Mol. Struct.* **2020**, *1210*, No. 128070.
(31) Lu, T.; Chen, F. Bond Order Analysis Based on the Laplacian of Electron Density in Fuzzy Overlap Space. *The Journal of Physical Chemistry A.* **2013**, *117*, 3100−3108.
(32) Marvel, C. S.; Moon, N. S. The Structure of Vinyl Polymers. VIII.1 Polystyrene and Some of its Derivatives. *J. Am. Chem. Soc.* **1940**, *62* (1), 45−49.
(33) Charlesby, A. Investigation of halo patterns of amorphous polymers. *J. Polym. Sci.* **1953**, *10* (2), 201−211.
(34) Katz, J. R. X-ray spectrography of polymers and in particular those having a rubber-like extensibility. *Trans. Faraday Soc.* **1936**, *32*, 77−94.
(35) Krimm, S.; Tobolsky, A. V. Quantitative X-Ray Studies of Order in Amorphous and Crystalline Polymers: Scattering from Various Polymers and a Study of the Glass Transition in Polystyrene and Polymethyl Methacrylate. *Textile Research Journal.* **1951**, *21* (11), 805.
(36) Tonoue, R.; Katsura, M.; Hamamoto, M.; Bessho, H.; Nakashima, S. A Method to Obtain the Absorption Coefficient Spectrum of Single Grain Coal in the Aliphatic C−H Stretching Region Using Infrared Transflection Microspectroscopy. *Appl. Spectrosc.* **2014**, *68* (7), 733.
(37) Sanjay, V.; Rajashekara, K. M.; Pattar, V.; Murugendrappa, M. V. Effect on electrical and dielectric properties of Te nanoparticle-doped PVA composite. *Journal of Materials Science: Materials in Electronics.* **2022**, *33*, 17382−17394.
(38) Talik, P.; Moskal, P.; Proniewicz, L. M.; Wesełucha-Birczyńska, A. The Raman spectroscopy approach to the study of Water−Polymer interactions in hydrated hydroxypropyl cellulose (HPC). *J. Mol. Struct.* **2020**, *1210*, No. 128062.
(39) Lin, S.; Peng, D.; Yang, W.; Gu, F.; Lan, Z. Theoretical studies on triplet-state driven dissociation of formaldehyde by quasi-classical molecular dynamics simulation on machine-learning potential energy surface. *The Journal of Chemical Physics.* **2021**, *155*, No. 214105.
(40) Veronezi, G. M. B.; Felisbino, M. B.; Gatti, M. S. V.; Mello, M. L. S.; Vidal, B. C. DNA Methylation Changes in Valproic Acid-Treated HeLa Cells as Assessed by Image Analysis, Immunofluor-


https://doi.org/10.1021/acsomega.4c04407
*ACS Omega* 2024, 9, 38668−38677

escence and Vibrational Microspectroscopy. *PLoS One.* **2017**, *12*, No. e0170740.
(41) Wu, J.; Chen, T.; Luo, X.; Han, D.; Wang, Z.; Wu, J. TG/FTIR analysis on co-pyrolysis behavior of PE, PVC and PS. *Waste Management.* **2014**, *34*, 676−682.
(42) Singh, R. K.; Ruj, B.; Sadhukhan, A. K.; Gupta, P. A TG-FTIR investigation on the co-pyrolysis of the waste HDPE, PP, PS and PET under high heating conditions. *Journal of the Energy Institute.* **2020**, *93*, 1020−1035.
(43) Egusa, S.; Ishigure, K.; Tabata, Y. Fast Neutron Irradiation Effects on Polymers. 2. Cross-Linking and Degradation of Polystyrene. *Macromolecules.* **1980**, *13*, 171−176.
(44) Gafar, S. M.; Abdel-Kader, N. M. Dosimetric characteristics and applications of cross-linking and degradation of a natural biopolymer Gum Acacia. *Radiochimica Acta.* **2020**, *108*, 223−229.
(45) Tomaz, V. A.; Rubira, A. F.; Silva, R. Solid-state polymerization of EDTA and ethylenediamine as one-step approach to monodisperse hyperbranched polyamides. *RSC Advances.* **2016**, *6*, 40717−40723.
(46) Maharana, T.; Negi, Y. S.; Mohanty, B. Review article: Recycling of polystyrene. *Polymer-Plastics Technology and Materials.* **2007**, *46*, 729−736.
(47) Kim, Y. S.; Hwang, G. C.; Bae, S. Y.; Yi, S. C.; Moon, S. K.; Kumazawa, H. Pyrolysis of polystyrene in a batch-type stirred vessel. *Korean Journal of Chemical Engineering.* **1999**, *16*, 161−165.
(48) Zhibo, Z.; Nishio, S.; Morioka, Y.; Ueno, A.; Ohkita, H.; Tochihara, Y.; Mizushima, T.; Kakuta, N. Thermal and chemical recycle of waste polymers. *Catalysis Today.* **1996**, *29*, 303−308.
(49) Gabdulkhakov, R. R.; Rudko, V. A.; Povarov, V. G.; Ugolkov, V. L.; Pyagay, I. N.; Smyshlyaeva, K. I. Technology of Petroleum Needle Coke Production in Processing of Decantoil with the Use of Polystyrene as a Polymeric Mesogen Additive. *ACS Omega* **2021**, *6* (30), 19995−20005.
(50) Guyot, A. Recent developments in the thermal degradation of polystyrene—A review. *Polym. Degrad. Stab.* **1986**, *15*, 219−235.


https://doi.org/10.1021/acsomega.4c04407
*ACS Omega* 2024, 9, 38668−38677